Control of Static VAR Compensator (SVC) With DC Voltage Regulation and Fast Dynamics By Feedforward and Feedback Loop

Guk C. Cho, Gu H. Jung,* Nam S. Choi** and Gyu H. Cho**

* *Department of Electrical Engineering*
Korea Advanced Institute of Science and Technology
373-1, Kusong-Dong, Yusong-Gu, Taejon, 305-701, Korea
Phone : 82-42-869-3424 Fax : 82-42-869-3410

** *Department of Electrical Engineering*
Yosu National Fisheries University
190, Guk-Dong, Yosu-City, Chonnam, 550-749, Korea
Phone : 82-662-40-6330 Fax : 82-662-41-7077

ABSTRACT : *This paper proposes a new control method of static var compensator (SVC) with three-level inverter to control reactive power with fast dynamics while maintaining DC side capacitor voltage constant. Firstly, using the circuit DQ-transformation, a general and simple model of SVC with three-level inverter is obtained, and DC and AC analyses are carried out to characterize the open-loop system. Based on the transfer function matrix of the system, modulation index control for reactive power compensation and phase angle control for DC side voltage regulation are designed. By inserting feedforward path to the voltage regulation loop the modulation index is successfully decoupled from the capacitor voltage whereby fast dynamics are achieved. The experimental results confirm the theoretical analyses and control method.*

I. INTRODUCTION

It is well known that there has been a large demand for high power/high voltage static var compensator (SVC) systems to regulate and stabilize transmission lines and to compensate industrial lagging loads. Various passive and active static var compensators have been reported in the literature [1].

Usually SVC's using forced commutated inverters have been made up of two-level voltage source inverters (VSI's) [2][3]. A neutral-point-clamped inverter (NPC inverter, also called three-level inverter) is reported in the literature [4]. The three-level inverter has the advantages that the blocking voltage of each switching device is one half of DC-link voltage and the harmonic contents of inverter output voltage are far less than those of two-level one at the same switching frequency. Thus three-level inverters can be operated at lower switching frequency without excessive harmonic contents and can be connected directly to 3.3kV AC mains using 4500V GTO's. These advantages enable the SVC system using three-level inverter to be suitable for large-scale reactive power compensation.

A new modelling method of SVC using three-level inverter is reported in the literature [5] by using the circuit DQ-transformation [6]. In [5], a general and simple equivalent DQ circuit of the presented SVC system is derived by eliminating the three-phase time varying nature of the system. Based on this general and simple model, in this paper, a new control method having fast dynamic response with DC side voltage regulation is presented and verified by experiment. To achieve fast dynamic response, reactive power is controlled by the modulation index of switching pattern while the DC side capacitor voltage is kept constant by controlling the phase angle 'α' of switching pattern simultaneously.

II. PRINCIPLES OF OPERATION

The block diagram of the SVC system presented in this paper is shown in Fig. 1. The SVC system consists of a three-level inverter, a set of linked reactors, DC-side capacitors, three-phase loads and the AC source.

The operating principles can be explained by considering the per-phase fundamental equivalent circuit of the SVC system. An equivalent inverter output voltage V_{oa1} is connected to the AC source V_{sa} through a linked reactor L and a resistor R_s representing the total losses in the inverter as shown in Fig. 2(a). Figs. 2(b) and 2(c) show the phasor diagram for leading (capacitive) and lagging (inductive) var generation, respectively. Fundamental reactive current is generated by voltage difference between V_{sa} and V_{oa1}. Thus, reactive power can be controlled from full leading (capacitive) to full lagging (inductive) by adjusting the amplitude

0-7803-2730-6/95 $4.00 © 1995 IEEE

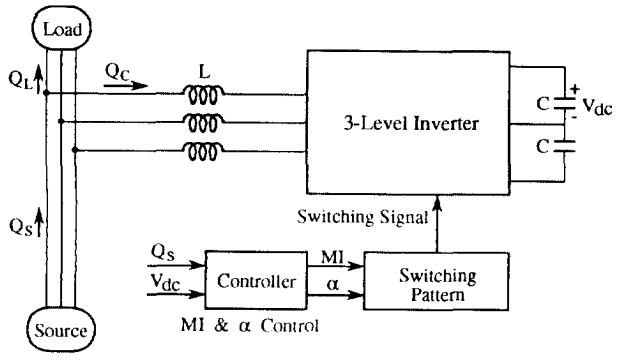

Fig. 1. Block diagram of the SVC system with 3-level inverter.

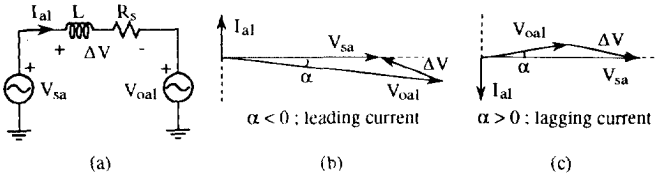

Fig. 2. (a) Per-phase fundamental equivalent circuit, (b) phasor diagram for providing leading vars, (c) phasor diagram for providing lagging vars; V_{sa}: line-to-neutral voltage of the source, V_{oa1}: fundamental component of the inverter output phase voltage, I_{a1}; fundamental component of line current.

of V_{oa1}. The inverter output voltage is given by

$$V_{oa1} = \frac{1}{\sqrt{2}} MI \cdot V_{dc} \tag{1}$$

where MI is the modulation index of pulse-width modulation (PWM) switching pattern of the inverter. It follows from (1) that V_{oa1} could be adjusted by two different ways. One is to change the DC side voltage V_{dc} indirectly with a fixed MI by controlling the phase angle α of V_{oa1} with respect to the AC source; this control method is well known as the phase angle control. In this paper, we suggest the other control method which is to change MI while the DC side voltage is kept constant by some means. Because the former depends closely on the dynamics of the DC side voltage, it has slower dynamic response than the latter which does not include the dynamics of the DC side voltage. A more detailed explanation is described in section V.

III. MODELLING

The simplified main circuit of SVC is shown in Fig. 3. By introducing so called circuit DQ-transformation method, a neat and instructive modelling of this circuit is presented in the literature [5]. For convenience, however, the modelling is reviewed in brief here. Modelling is carried out with the following assumptions:

1) all the switches are ideal,
2) the source voltages are balanced,
3) the total losses in the inverter are represented by equivalent resistor R_s,
4) the harmonic contents caused by switching action are negligible.

The original circuit is too complex to analyze, so it is partitioned into several basic sub-circuits as shown in Fig. 3. The three-phase source voltage ($\mathbf{v}_{s,abc}$) and synchronously rotating DQ transformation matrix **K** are defined as follows:

$$\mathbf{v}_{s,abc} = \begin{bmatrix} v_{sa} \\ v_{sb} \\ v_{sc} \end{bmatrix} = \sqrt{2/3}\, V_s \begin{bmatrix} \sin(\omega t) \\ \sin(\omega t - 2\pi/3) \\ \sin(\omega t + 2\pi/3) \end{bmatrix}, \tag{2}$$

$$\mathbf{K} = \sqrt{2/3} \begin{bmatrix} \cos(\omega t + \alpha) & \cos(\omega t - 2\pi/3 + \alpha) & \cos(\omega t + 2\pi/3 + \alpha) \\ \sin(\omega t + \alpha) & \sin(\omega t - 2\pi/3 + \alpha) & \sin(\omega t + 2\pi/3 + \alpha) \\ 1/\sqrt{2} & 1/\sqrt{2} & 1/\sqrt{2} \end{bmatrix}, \tag{3}$$

where the V_s and 'ω' denote the rms line-to-line voltage and the angular frequency of the source voltage, respectively, and the variable 'α' is the phase angle of the matrix **K**.

Under the assumption that the harmonic components caused by switching action in the inverter are negligible, a switching function **S** can be defined as follows:

$$\mathbf{S} = \begin{bmatrix} S_a \\ S_b \\ S_c \end{bmatrix} = \sqrt{2/3}\, d \begin{bmatrix} \sin(\omega t + \alpha) \\ \sin(\omega t - 2\pi/3 + \alpha) \\ \sin(\omega t + 2\pi/3 + \alpha) \end{bmatrix}. \tag{4}$$

Note that the matrix **K** synchronously rotates in phase with the switching function **S** and the amplitude, $\sqrt{2/3}\,d$, in (4) indicates the modulation index MI of the switching function **S**. A variable $\mathbf{x}_{abc}$ which denotes any AC voltages and currents on the abc-plane is transformed into $\mathbf{x}_{qdo}$ on the qd-axis by DQ transformation matrix **K**:

$$\mathbf{x}_{qdo} = \mathbf{K}\,\mathbf{x}_{abc}, \qquad \mathbf{x}_{abc} = \mathbf{K}^{-1}\mathbf{x}_{qdo}. \tag{5}$$

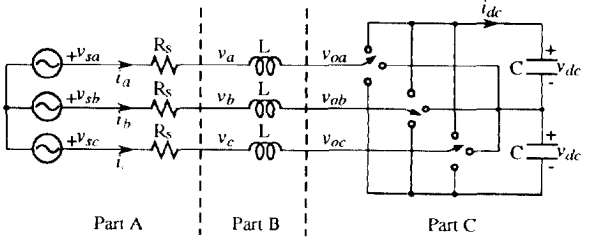

Fig. 3. Simplified main circuit of the SVC system.

Applying the transformation matrix **K** to all the circuit variables results in the equivalent circuit of each part as shown in Fig. 4. That is, the inductor set becomes a second order gyrator-coupled system and the switch set becomes a transformer as well. Then a simple and complete equivalent circuit is obtained as shown in Fig. 5 by combining simply the transformed parts of sub-circuits. Here, $\mathbf{v}_{s,qdo}$ is given by

$$\mathbf{v}_{s,qdo} = \mathbf{K}\mathbf{v}_{s,abc} = V_s \left[-\sin\alpha \quad \cos\alpha \quad 0\right]^T . \tag{6}$$

Since all switching harmonics are assumed to be negligible, if only the fundamental component is identical, the responses are just the same regardless of actual switching patterns.

IV. ANALYSES

From the equivalent circuit obtained in the previous section, DC analysis is done to know the steady state operation and AC analysis is carried out to find the transient characteristics of the system.

A. DC Analysis

In the steady state operation, the inductors seem to be short and the capacitor seems to be open and all the circuit variables imply DC values denoted by capital letters. The equivalent circuit for DC analysis is shown in Fig. 6. For a modulation index MI ($=\sqrt{2/3}D$) and a phase angle 'α' of switching pattern, the operating point is determined as follows:

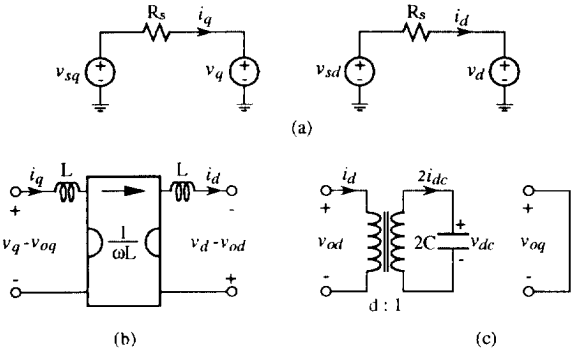

Fig. 4. Circuit DQ-transformed results (a) of Part A, (b) of Part B, (c) of Part C.

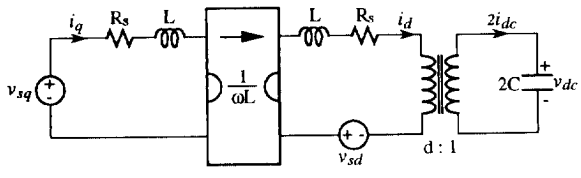

Fig. 5. Circuit DQ-transformed equivalent circuit of the SVC system.

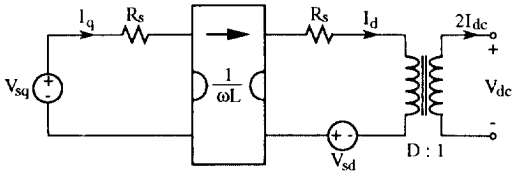

Fig. 6. DC equivalent circuit for the steady state analysis.

$$V_{sq} = -V_s \sin\alpha , \qquad V_{sd} = V_s \cos\alpha , \tag{7}$$

$$I_q = -\frac{V_s}{R_s}\sin\alpha , \qquad I_d = 0 , \tag{8}$$

$$V_{dc} = \frac{V_s}{D}\left[\cos\alpha - \frac{\omega L}{R_s}\sin\alpha\right] . \tag{9}$$

Therefore, the real power P_c and the reactive power Q_c drawn by the inverter system are expressed as:

$$P_c = V_{sq} I_q + V_{sd} I_d = \frac{V_s^2}{2R_s}\left\{1 - \cos(2\alpha)\right\} , \tag{10}$$

$$Q_c = V_{sq} I_d - V_{sd} I_q = \frac{V_s^2}{2R_s}\sin(2\alpha) . \tag{11}$$

The real power corresponds to the total losses in the inverter. Note that in the range of small α, i.e., $|\alpha| < 5^o$, the amount of reactive power is almost proportional to α. In the steady state, it can be seen from (9) and (11) that Q_c is dependent on only α and the voltage V_{dc} is dependent on both α and MI, i.e., D of switching pattern.

B. AC Analysis

The AC analysis is carried out by adding some perturbations to the control variables 'D' and 'α'. Therefore the circuit variables consist of DC and AC components and thus the perturbed component (AC value) is indicated by diacritical mark, $\hat{}$, of the corresponding variable to distinguish from the quiescent value. Also, the following assumptions are made:

1) the quiescent α is nearly zero,
2) the perturbed $\hat{\alpha}$ is small ($|\hat{\alpha}| < 5^o$),
3) the second order terms, i.e., products of variations, are negligible.

With the aforementioned assumptions, we obtain

$$\hat{v}_{sq} = -V_s \sin(\alpha+\hat{\alpha}) + V_s \sin\alpha \approx -V_s \hat{\alpha} , \tag{12}$$

$$\hat{v}_{sd} = V_s \cos(\alpha+\hat{\alpha}) - V_s \cos\alpha \approx 0 , \tag{13}$$

$$\hat{v}_{od} = (D+\hat{d})(V_{dc}+\hat{v}_{dc}) - D\,V_{dc} \approx V_{dc}\,\hat{d} + D\,\hat{v}_{dc} , \tag{14}$$

$$2\hat{i}_{dc} = (D+\hat{d})\,\hat{i}_d \approx D\,\hat{i}_d , \tag{15}$$

$$\hat{Q}_c = (v_{sq} i_d - v_{sd} i_q) - (V_{sq} I_d - V_{sd} I_q) \approx -V_s \hat{i}_q . \tag{16}$$

Therefore, the resultant small signal equivalent circuit can be drawn as shown in Fig. 7, where all the DC components are eliminated. Now it is straightforward to get the state equation of the system. The inputs of the system are the control variables $\hat{d}$ and $\hat{\alpha}$, and the outputs are the generated reactive power $\hat{Q}_c$ and the capacitor voltage $\hat{v}_{dc}$. From Fig. 7, we have

$$\frac{d\mathbf{x}}{dt} = \mathbf{A}\mathbf{x} + \mathbf{B}\mathbf{u} , \tag{17}$$

$$\mathbf{y} = \mathbf{C}\mathbf{x} , \tag{18}$$

where

$$\mathbf{x} = \begin{bmatrix} \hat{i}_q & \hat{i}_d & \hat{v}_{dc} \end{bmatrix}^T , \quad \mathbf{u} = \begin{bmatrix} \hat{d} & \hat{\alpha} \end{bmatrix}^T , \quad \mathbf{y} = \begin{bmatrix} \hat{Q}_c & \hat{v}_{dc} \end{bmatrix}^T , \tag{19}$$

$$\mathbf{A} = \begin{bmatrix} -R_s/L & -\omega & 0 \\ \omega & -R_s/L & -D/L \\ 0 & D/2C & 0 \end{bmatrix} , \quad \mathbf{B} = \begin{bmatrix} 0 & -V_s/L \\ -V_{dc}/L & 0 \\ 0 & 0 \end{bmatrix} , \tag{20}$$

$$\mathbf{C} = \begin{bmatrix} -V_s & 0 & 0 \\ 0 & 0 & 1 \end{bmatrix} . \tag{21}$$

Therefore, we obtain

$$\begin{bmatrix} \hat{Q}_c(s) \\ \hat{v}_{dc}(s) \end{bmatrix} = \mathbf{G}_p(s) \begin{bmatrix} \hat{d}(s) \\ \hat{\alpha}(s) \end{bmatrix} , \tag{22}$$

where $\mathbf{G}_p(s)$ is the transfer function matrix of the system given by

$$\mathbf{G}_p(s) = \mathbf{C}(s\mathbf{I} - \mathbf{A})^{-1}\mathbf{B} = \frac{1}{M(s)} \begin{bmatrix} N_1(s) & N_2(s) \\ N_3(s) & N_4(s) \end{bmatrix} , \tag{23}$$

where

$$M(s) = s^3 + \frac{2R_s}{L}s^2 + \left\{ \left[\frac{R_s}{L} \right]^2 + \frac{D^2}{2LC} + \omega^2 \right\} s + \frac{D^2 R_s}{2L^2 C} , \tag{24}$$

$$N_1(s) = -\frac{\omega V_s V_{dc}}{L} s , \tag{25}$$

$$N_2(s) = \frac{V_s^2}{L} \left[s^2 + \frac{R_s}{L}s + \frac{D^2}{2LC} \right] , \tag{26}$$

$$N_3(s) = -\frac{D V_{dc}}{2LC} \left[s + \frac{R_s}{L} \right] , \tag{27}$$

$$N_4(s) = -\frac{\omega D V_s}{2LC} . \tag{28}$$

Eq. (22) leads to the block diagram of the open loop SVC system for small signal as shown in Fig. 8. Based on the transfer function matrix $\mathbf{G}_p(s)$ in (23), the step responses of the outputs are simulated with the circuit parameters given in Table I. Figs. 9 and 10 show the step responses of the outputs for step changes of $\hat{d}$ and $\hat{\alpha}$, respectively.

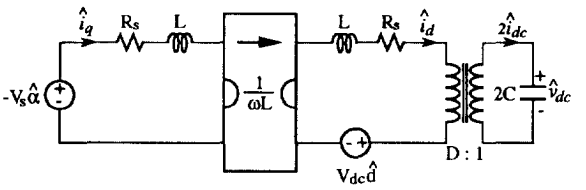

Fig. 7. Equivalent circuit for the small signal.

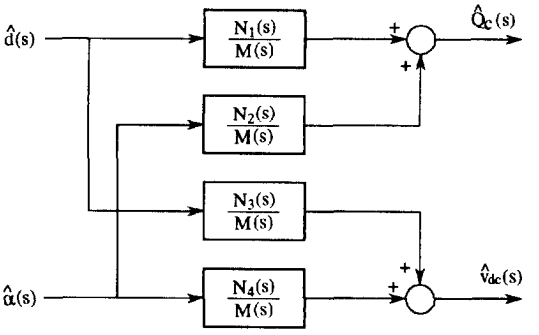

Fig. 8. Block diagram of the open loop SVC system.

Table I. Circuit Parameters.

meaning	symbol	value
fundamental frequency	f	60 [Hz]
fundamental angular frequency	ω	2πf [rad/sec]
rms line-to-line source voltage	V_s	220 [V]
effective resistance	R_s	0.3 [Ω]
linked reactor	L	6 [mH]
DC-side capacitor	C	2200 [μF]

V. CONTROLLER DESIGN

The modelled plant is a multi-input and multi-output (MIMO) system which has two inputs and two outputs. The inputs are the modulation index ($\hat{d}$) and the phase angle ($\hat{\alpha}$) of switching pattern, and the outputs are the reactive power ($\hat{Q}_c$) and the capacitor voltage ($\hat{v}_{dc}$).

As mentioned in section II, to compensate the required reactive power there are two different ways in adjusting the inverter output voltage V_{oa1}. One is to change the capacitor voltage V_{dc} with a fixed MI, and the other is to change MI, i.e., d, with a fixed V_{dc}. In the former case, the $\hat{d}$ is zero due to the fixed MI and thus the plant becomes single-input ($\hat{\alpha}$) and single-output ($\hat{Q}_c$) system which can be obtained from Fig. 8. Fig. 11(a) shows the block diagram of closed loop system for this case. In the latter case, as shown in Fig. 11(b) two feedback loops may be required, if separate fixed DC voltage source is not employed. One is the MI control loop to generate the required reactive power and the other is the phase angle control loop to keep the DC capacitor voltage constant. The former control method depends closely on the

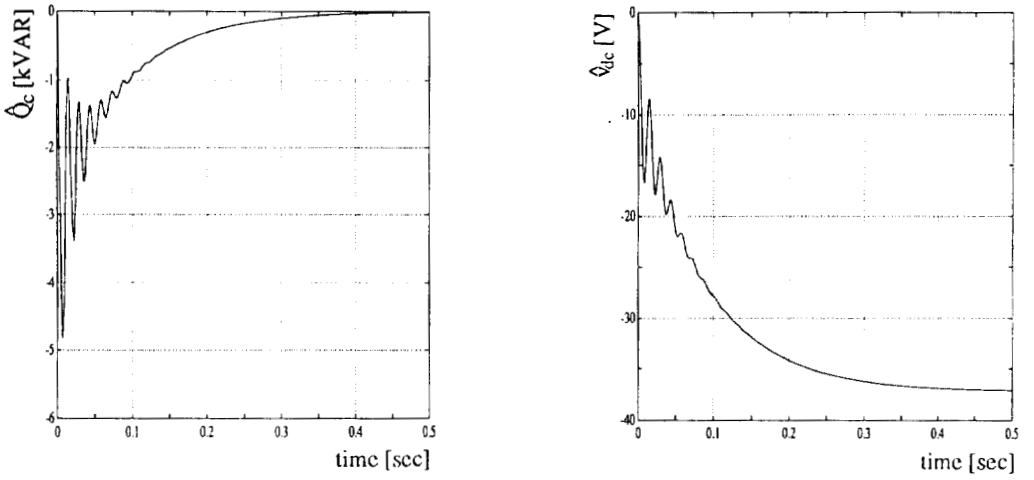

(a) (b)

Fig. 9. Step responses of (a) $\hat{Q}_c$ and (b) $\hat{v}_{dc}$ for step change of input $\hat{d}$ ($\hat{d} = \sqrt{3/2} \cdot 0.2$).

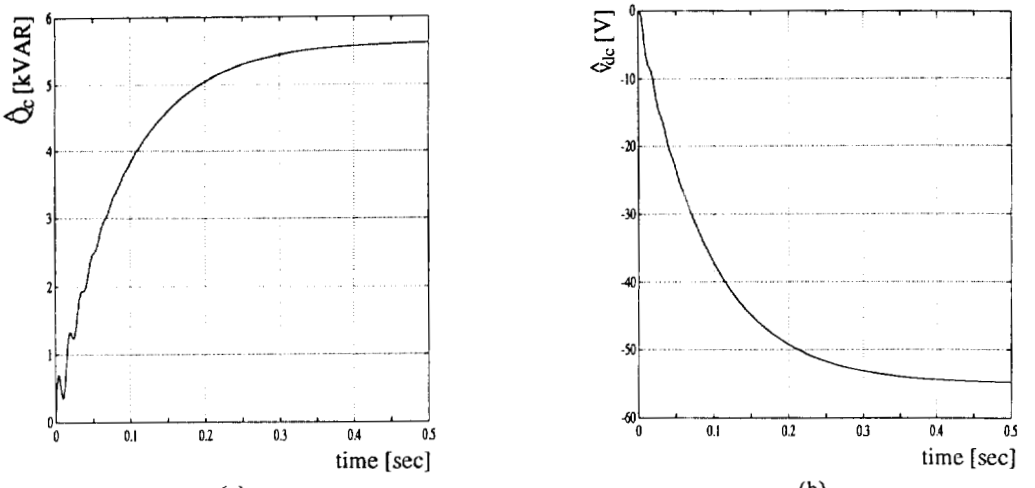

(a) (b)

Fig. 10. Step responses of (a) $\hat{Q}_c$ and (b) $\hat{v}_{dc}$ for step change of input $\hat{\alpha}$ ($\hat{\alpha} = 2[deg.]$).

dynamics of the DC capacitor voltage V_{dc} and thus has slower dynamic response than the latter one which is not dependent on the voltage V_{dc}. Even for the latter one, however, it is not easy to achieve fast dynamic response with just two feedback loops as shown in Fig. 11(b). Because when the MI is controlled to generate the required reactive power, the regulated DC capacitor voltage may deviate from its fixed value in the transient state.

To achieve fast dynamic response of reactive power compensation the capacitor voltage v_{dc} should be kept constant even in the transient state. From (22), we have

$$\hat{Q}_c(s) = \frac{1}{M(s)} \left\{ N_1(s)\hat{d}(s) + N_2(s)\hat{\alpha}(s) \right\} , \tag{29}$$

$$\hat{v}_{dc}(s) = \frac{1}{M(s)} \left\{ N_3(s)\hat{d}(s) + N_4(s)\hat{\alpha}(s) \right\} . \tag{30}$$

In order to make the capacitor voltage constant in the transient state, the numerator of right-hand side of (30) must be zero. Therefore,

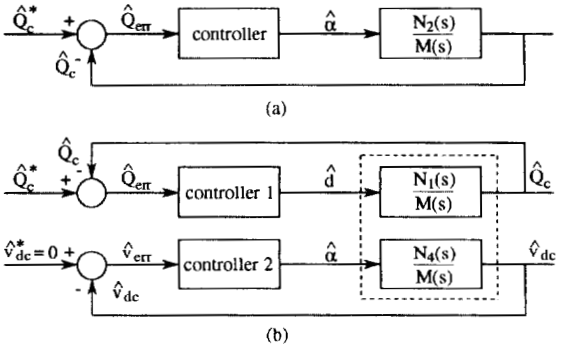

Fig. 11. Two different control methods to generate the required reactive power; (a) phase angle α control method, (b) modulation index MI and phase angle α control method.

$$\hat{\alpha}(s) = -\frac{V_{dc}}{\omega V_s}(s + R_s/L)\hat{d}(s) . \tag{31}$$

By substituting (31) in (29), we obtain

$$\hat{Q}_c(s) = -\frac{V_s V_{dc}}{\omega L}\hat{d}(s) . \tag{32}$$

Based on these equations a new control method is suggested consisting of two feedback controllers having one feedforward path as shown in Fig. 12. The modulation index control loop is constructed by using PI controller to generate the required reactive power. Feedback loop and the feedforward path given by (31) are constructed so as to keep the capacitor voltage constant in the steady state and the transient state as well. By adding the feedforward path, the modulation index is successfully decoupled from the DC side voltage. The control parameters can be designed by using root-locus technique.

VI. EXPERIMENTAL RESULTS

To confirm the validity of the presented analyses and control method, an experimental 5kVA prototype is implemented and tested. A three-phase three-level inverter is constructed with the values given in Table I.

Supposing the application of high power operation, the switching frequency at each active device is chosen to be relatively low so as to meet the switching characteristics of the gate turn-off thyristor (GTO) devices. In order to reduce the harmonic current factor (HCF) of the PWM switching patterns, optimal three-level PWM patterns are employed. The optimal PWM switching angles used in this experiment are shown in Fig. 13 and stored in EPROM memory. The switching frequency of each switching device is 180Hz.

Figs. 14 and 15 show the step responses of the outputs of the open loop system for step changes of $\hat{d}$ and $\hat{\alpha}$, respectively. To check the validity of the presented analyses, the step responses of the open loop system are compared with the simulated ones as shown in Figs. 9 and 10. The close agreements among one another prove the usefulness of the analyses.

Fig. 16 shows the block diagram of the overall closed loop system with the proposed control method, where the DC capacitor voltage is regulated to 210[V]. The control parameters are determined by using MATLAB tool as follows:

$$K_{pQ} = -1 \times 10^{-5}, \qquad K_{iQ} = -5 \times 10^{-3}, \tag{33}$$

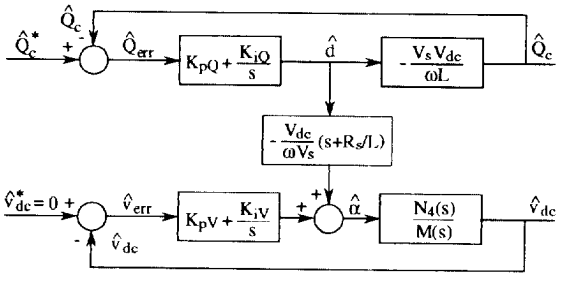

Fig. 12. Proposed new control method with feedback and feedforward path.

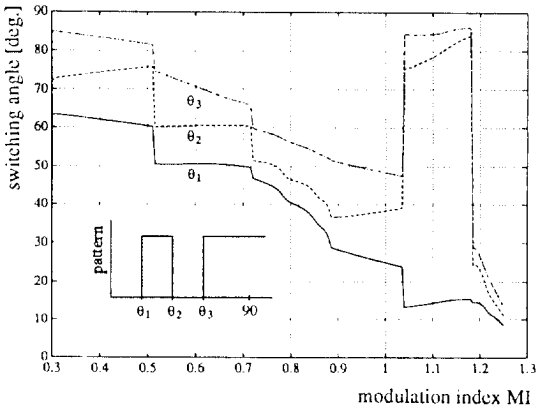

Fig. 13. Optimal PWM switching angles for 3-level vs. MI.

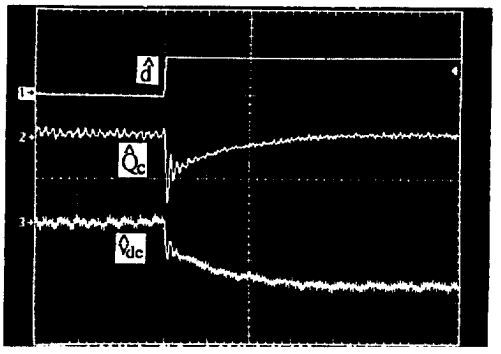

Fig. 14. Step responses for step change of input $\hat{d}$ ($\hat{d} = \sqrt{3/2} \cdot 0.2$); Ch1: $\hat{d}$, Ch2: reactive power $\hat{Q}_c$, 6kVAR/div., Ch3: DC capacitor voltage $\hat{v}_{dc}$, 20V/div., 100ms/div.

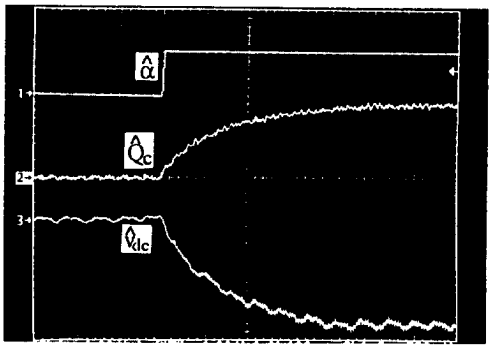

Fig. 15. Step responses for step change of input $\hat{\alpha}$ ($\hat{\alpha} = 2[deg.]$); Ch1: $\hat{\alpha}$, Ch2: reactive power $\hat{Q}_c$, 6kVAR/div., Ch3: DC capacitor voltage $\hat{v}_{dc}$, 20V/div., 100ms/div.

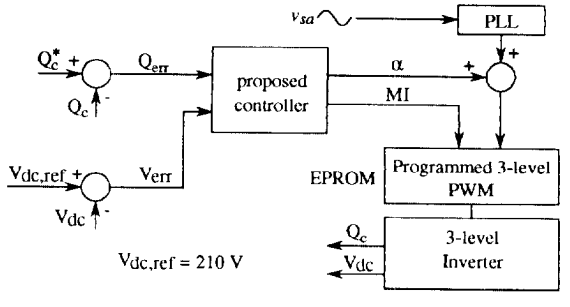

Fig. 16. Block diagram of the overall closed loop system with the proposed control method.

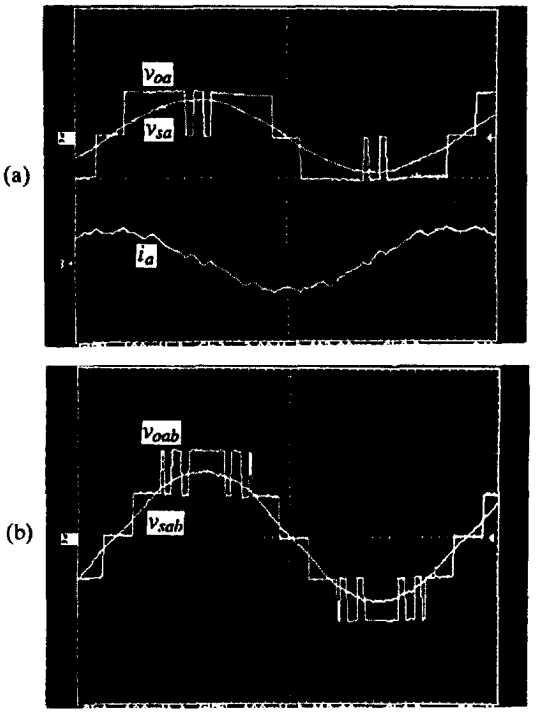

Fig. 17. Capacitive var generation for $Q_c^* = -5kVAR$; (a) Source phase voltage v_{sa}, 200V/div., inverter output phase voltage v_{oa}, 200V/div., and line current i_a, 25A/div., 2ms/div., (b) Source line-to-line voltage v_{sab}, 200V/div. and inverter output line-to-line voltage v_{oab}, 200V/div., 2ms/div.

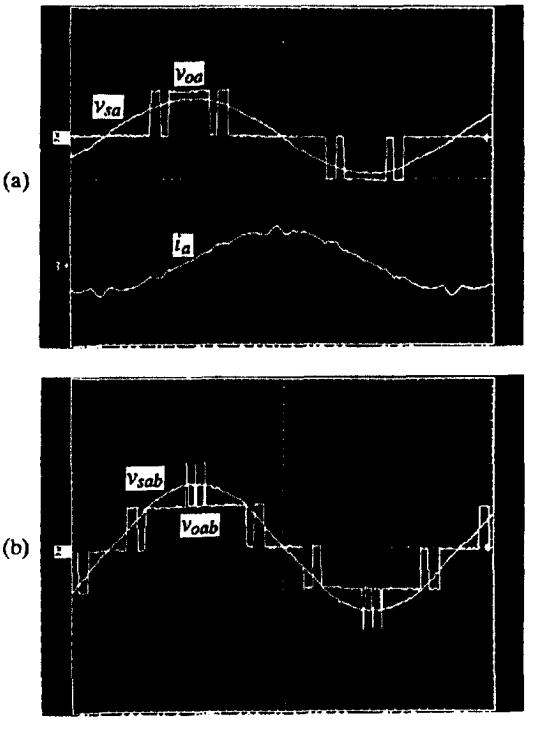

Fig. 18. Inductive var generation for $Q_c^* = 5kVAR$; (a) Source phase voltage v_{sa}, 200V/div., inverter output phase voltage v_{oa}, 200V/div., and line current i_a, 25A/div., 2ms/div., (b) Source line-to-line voltage v_{sab}, 200V/div. and inverter output line-to-line voltage v_{oab}, 200V/div., 2ms/div.

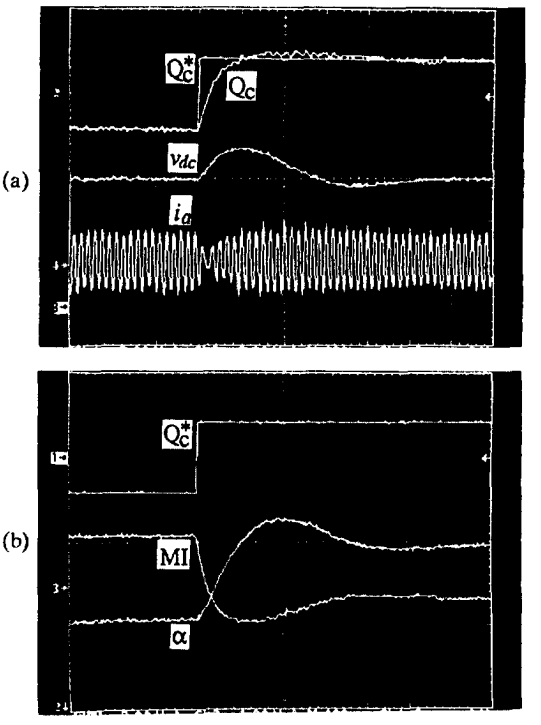

Fig. 19. Transient response without feedforward path for a step change of Q_c^* from $-5kVAR$ to $+5kVAR$; (a) Ch1: Reactive power command Q_c^*, Ch2: generated reactive power Q_c, 6kVAR/div., Ch3: regulated DC capacitor voltage v_{dc}, 70V/div., Ch4: line current i_a, 25A/div., 100ms/div., (b) Ch1: Q_c^*, 6kVAR/div., Ch2: modulation index MI, 0.25/div., Ch3: phase angle α, 2^o/div., 100ms/div.

$$K_{pV} = -2 \times 10^{-3}, \qquad K_{iV} = -3 \times 10^{-2}. \tag{34}$$

Fig. 17 shows the steady state results for the capacitive var generation; the var command Q_c^* is -5kVAR. Fig. 18 shows the steady state results for the inductive var generation. Figs. 17(a) and 18(a) show the source phase voltage v_{sa}, the inverter output phase voltage v_{oa} and AC line current i_a for the capacitive and inductive var generation, respectively. Figs. 17(b) and 18(b) show the AC line-to-line voltage v_{sab} and the inverter output line-to-line voltage v_{oab}. The modulation index MI of the switching pattern is increased for capacitive and decreased for inductive var generation, whereas the phase angle α of the inverter output voltage becomes negative for capacitive and positive for inductive var generation. It is worthy to note that the line currents generated by the three-level inverter have low harmonic components even though the switching frequency of the active device is 180Hz.

Fig. 19 shows the transient response of the SVC system without inserting the feedforward path for a step change in the var command. As shown in Fig. 19, the coupling between MI and v_{dc} causes the large deviation of the DC capacitor voltage and thus the responses are not satisfactory. Figs. 20 and 21 show the transient

responses of the SVC system with the feedforward path for a step change in the var command Q_c^* from capacitive to inductive and vice versa. As shown in Figs. 20(a) and 21(a), the capacitor voltage is regulated well and thus the required reactive power is generated nearly in about one cycle, 20msec. This implies that the deviation of DC side capacitor voltage could be suppressed by the feedforward control of (31). The modulation index (MI) and the phase angle (α) controlled by two-PI and one-feedforward controller are shown in Figs. 20(b) and 21(b), respectively.

VII. CONCLUSION

The general and simple DQ-transformed equivalent circuit for the presented SVC system is obtained and analyzed completely including DC and AC characteristics. The open loop transfer function matrix is obtained from the analyses of the DQ-transformed equivalent circuit. Based on the transfer function matrix, the var controller is designed so as to achieve fast dynamic response of reactive power compensation while the DC side voltage v_{dc} remains constant. This is done by controlling the modulation index of the switching function for the generation of the required reactive power and controlling the phase angle α for the DC side voltage regulation, simultaneously. By means of adding feedforward path to the voltage regulation loop the modulation index is successfully decoupled from the DC side voltage. Therefore, the DC side voltage is regulated well and thus the required reactive power is generated nearly in about one cycle. The experimental results confirm the validity of the proposed analyses and control method of SVC system.

REFERENCE

[1] L. Gyugyi, "*Reactive Power Generation and Control by Thyristor Circuits,*" IEEE Trans. Ind. Appl., vol. IA-15, no. 5, pp. 521-532, Sept./Oct., 1979.

[2] L. Moran, P. Ziogas and G. Joos, "*Analysis and Design of a 3-ϕ Synchronous Solid-State Var Compensator,*" IEEE Trans. Ind. Appl., vol. IA-25, no. 4, pp. 598-608, July/Aug., 1989.

[3] Hassan Ali Kojori, Shashi B. Dewan and J. Douglas Lavers, "*A Large-Scale PWM Solid-State Synchronous Condenser,*" IEEE Trans. Ind. Appl., vol. IA-28, no. 1, pp. 41-49, Jan./Feb., 1992.

[4] Akira Nabae, Isao Takahashi and Hirofumi Akagi, "*A New Neutral-Point-Clamped PWM Inverter,*" IEEE Trans. Ind. Appl., vol. IA-17, no. 5, pp. 518-523, Sept./Oct., 1981.

[5] Guk C. Cho, Nam S. Choi, Chun T. Rim and Gyu H. Cho, "*Modeling, Analysis and Control of Static VAR Compensator Using 3-Level Inverter,*" IEEE Ind. Appl. Society Annual Meeting, pp. 837-843, 1992.

[6] Chun T. Rim, Dong Y. Hu and Gyu H. Cho, "*Transformers as Equivalent Circuits of Switches: General Proofs and DQ Transformation-Based Analyses,*" IEEE Trans. Ind. Appl., vol. IA-26, no. 4, pp. 777-785, July/Aug., 1990.

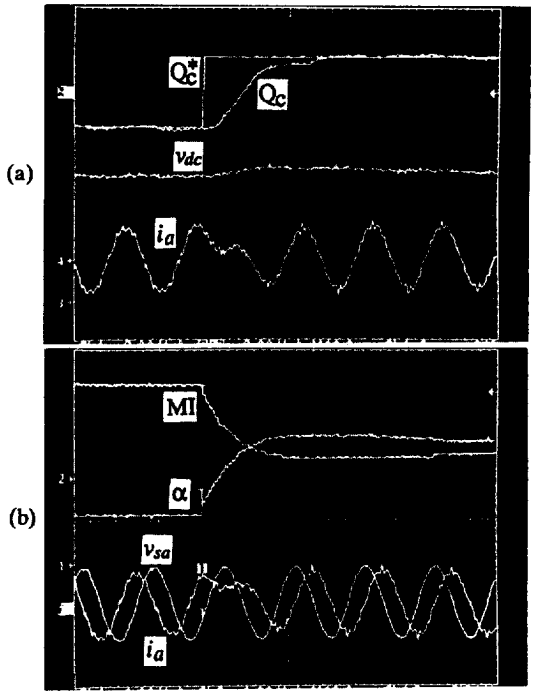

Fig. 20. Transient response with feedforward path for a step change of Q_c^* from $-5kVAR$ to $+5kVAR$; (a) Ch1: Reactive power command Q_c^*, Ch2: generated reactive power Q_c, 6kVAR/div., Ch3: regulated DC capacitor voltage v_{dc}, 70V/div., Ch4: line current i_a, 25A/div., 10ms/div., (b) Ch1: Modulation index MI, 0.25/div., Ch2: phase angle α, 2^o/div., Ch3: source phase voltage v_{sa}, 200V/div., Ch4: i_a, 25A/div., 10ms/div.

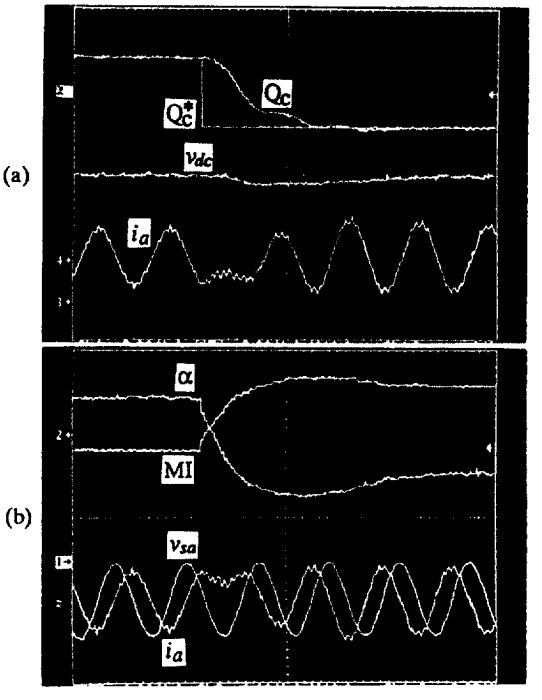

Fig. 21. Transient response with feedforward path for a step change of Q_c^* from $5kVAR$ to $-5kVAR$; (a) Ch1: Reactive power command Q_c^*, Ch2: generated reactive power Q_c, 6kVAR/div., Ch3: regulated DC capacitor voltage v_{dc}, 70V/div., Ch4: line current i_a, 25A/div., 10ms/div., (b) Ch1: Modulation index MI, 0.25/div., Ch2: phase angle α, 2^o/div., Ch3: source phase voltage v_{sa}, 200V/div., Ch4: i_a, 25A/div., 10ms/div.